Desalination and Water Treatment
www.deswater.com

doi:10.5004/dwt.2019.23369

142 (2019) 308–320
February

Efficient removal of azo dyes from water with chitosan/carbon nanoflower as a novel nanocomposite synthesized by pyrolysis technique

Mahboubeh Kafil[a,b,*], Saeed Boroomand Nasab[b], Hadi Moazed[b], Jorma Jokiniemi[a], Anna Lähde[a], Amit Bhatnagar[a]

[a]*Department of Environmental and Biological Sciences, University of Eastern Finland, FI-70211 Kuopio, Finland, Tel. +358 414708731; emails: makafil@uef.fi, m-kafil@phdstu.scu.ac.ir (M. Kafil), Tel. +358 40 5050668; email: jorma.jokiniemi@uef.fi (J. Jokiniemi), Tel. +358 40 3553805; email: anna.lahde@uef.fi (A. Lähde), Tel. +358 50 3696419; email: amit.bhatnagar@uef.fi (A. Bhatnagar)*
[b]*Department of Irrigation and Drainage Engineering, Faculty of Water Sciences Engineering, Shahid Chamran University of Ahvaz, Khuzestan, Iran, Tel. +98 9161183014; emails: boroomand@scu.ac.ir, boroomandsaeed@yahoo.com (S.B. Nasab), hmoazed955@yahoo.com (H. Moazed)*

Received 4 May 2018; Accepted 28 October 2018

ABSTRACT

In this study, chitosan/carbon nanoflowers as a novel nanocomposite were synthesized via spray pyrolysis technique for dye removal from water. To examine the characteristics of pure and dye-loaded nanocomposite, field emission scanning electron microscopy, zeta potential, and Fourier transform infrared spectroscopy analyses were performed. The adsorption studies were conducted in batch mode for the removal of two azo dyes, Acid Black1 (AB1) and Congo red (CR), from aqueous solution. The effect of principal factors such as solution pH, contact time, adsorbent dosage, temperature, initial dye concentration, and ionic strength on dye adsorption was optimized. The equilibrium was found to be achieved in 60 min at 25°C, and the pseudo-second-order model provided the best fit to the experimental data. Maximum adsorption capacities of AB1 and CR were found to be 259.13 and 553.12 mg g^{-1}, respectively (according to Langmuir model under initial dye concentration of 400 mg L^{-1} at pH = 6.75).

Keywords: Nanocomposites; Carbon nanoflowers; Chitosan; Adsorption; Azo dyes

1. Introduction

With the excessive speed of industrialization and growing rate of population, contamination of water resources is unavoidable [1]. Dye-containing wastewaters are discharged into the environment from different dye stuff manufacturing industries (such as textile, paper and pulp, electroplating, tannery, food, cosmetic, and pharmaceuticals) [2–4]. These effluents have aesthetic problems, and most of them are toxic, mutagenic, and carcinogenic, which have negative impact on public health and aquatic life [3–7]. Azo dyes, most versatile category of synthetic organic colorants, are heavily used by textile industry and contain one or more azo groups (–N=N–) with aromatic ring, substituted by sulfonate groups. They have special stability, low reactivity, and biodegradability that make wastewater difficult to treat under aerobic conditions [5–9]. Also, their chemical stability and versatility make them the largest group of dyes which constitutes 60%–70% of all dyes [9].

For the removal of dyes from wastewater, a number of technologies including ion exchange [6,10], chemical oxidation [11], and adsorption [3] have been employed. However, adsorption process is regarded as one of the promising alternative treatments due to the ease of operation, high efficiency, and low energy requirement [1]. Various adsorbents such as activated carbon [12,13], sepiolite [14], vermiculite [15], and magnetic carbon nanotubes [16–19] have been successfully used to remove dyes from water.

* Corresponding author.

Chitosan (CS) is characterized as a biodegradable and nontoxic biomaterial which has shown excellent adsorption capacity for anionic dyes [20,21]. This is attributed to the presence of active amine (–NH_2) groups and hydroxyl groups in its monomers [22]. However, because of weak mechanical properties and low specific gravity of CS, several attempts have been made to produce more effective adsorbents [21,23].

Functional groups have significant impact on adsorption properties of carbon-nanobased materials (carbon nanoflowers (CNF)) because the wettability of their surface can be changed by functional groups, which make them more hydrophilic and suitable for the adsorption of polar compounds. However, functional groups may enhance diffusion resistance and make their internal space less attainable [18]. To remove these functional groups, the materials are exposed to high temperatures under vacuum [18]. One drawback of using CNFs is their insolubility and aggregation tendency in aqueous solutions. Modification of CNFs with polymers is a promising solution for this problem. Some of these materials include polystyrene sulfonate, CS, and polyvinylpyrrolidene [24]. On the other hand, decoration of CNFs with polymers may combine unique properties of two materials together [25].

The synthesis of particles with aerosol is a one-step continuous process, producing particles in the range of 1–5 μm size. Besides this, it has good control on particle size distribution [26]. Spray pyrolysis produces powders which have superior characteristics including more crystalline nature and less aggregation tendency which make them a superior adsorbent compared with powders made by conventional methods like liquid-phase precipitation [27]. The aerosol method is used in the production of oxides, metal oxides [26], and inhalation particles [27].

In this study, the potential of CS/CNFs composite, synthesized by spray pyrolysis method, was examined for the removal of two azo dyes, Acid Black1 (AB1) and Congo red (CR), from aqueous solutions. The experiments were conducted in batch mode under different experimental conditions. To deduce the adsorption mechanisms, kinetic and equilibrium models were applied to the experimental data.

2. Materials and methods

2.1. Chemicals

Preceramic silicon-carbon, CS, acetic acid, and sodium dodecyl sulphate (SDS, applied as a surfactant) were used for synthesis of CS/CNFs with spray pyrolysis. The chemicals were purchased from Sigma-Aldrich, Finland. AB1 and CR with chemical formulae of $C_{32}H_{22}N_6Na_2O_6S_2$ and $C_{22}H_{14}N_6Na_2O_9S_2$ and molecular weight of 616.49 and 696.66 g mol^{-1} with 96% and 99.99% purity, respectively, were also purchased from Sigma-Aldrich, Finland. The chemicals used for the experiments were of analytical reagent grade.

2.2. Synthesis of CNFs

CNFs were produced as previously described by Miettinen et al. [28]. Briefly, preceramic silicon-carbon particles were annealed in argon at atmospheric pressure, and the temperature was increased from 1,900°C to 2,600°C which resulted in the transformation of amorphous Si–C core into CNFs. This graphene sheet composite consisted of curved carbon layers with diameter lower than 60 nm. The core in the carbon structure, which is detectable at 1,900°C, reduced with the increase in temperature and disappeared completely at 2,200°C [29].

2.3. Spray pyrolysis of CS/CNFs

In the first step, CS stock solution was prepared by mixing 1.25 g of CS in 2.5 mL of acetic acid (0.5%) and diluted with 500 mL of deionized water. CS/CNF stock solution was prepared by dissolving 0.25 g of CNFs to 500 mL of CS stock solution in the presence of 50 mg SDS. The stock solution was atomized with an ultrasonic nebulizer (RBI Pyrosol 7901). The droplets were suspended in the N_2 carrier gas at the flow rate of 1.5 L min^{-1} (T = 22°C, p = 101.3 kPa) and carried to the heated zone of the reactor. The temperature of the heated zone was kept at 200°C, and dry particles were formed by evaporation of the solvent. The flow Reynolds number was 49, indicating fully laminar flow field, and the residence time was 10 s. The aerosol exiting the heated zone of the reactor was diluted and cooled down with dry air at ambient temperature using a porous tube diluter (sintered metal tube with pore size of 20 μm) [26,30]. The flow rate was 27.5 L min^{-1}. The dilution caused a rapid quenching of any potential reactions, prevented the recondensation of gaseous species, and decreased the wall deposition losses of the dry particles. The dry particles were collected on the filters (Pall Corp. (New York), 47 mm, Zefluor 1 μm).

To analyze the changes in functional groups of nanocomposite before and after dye adsorption, Fourier transform infrared (FTIR) analysis was conducted in the range of 400–4,000 cm^{-1} with Thermonicolet 8,700. The size and shape of the particles were studied with a scanning electron microscope (SEM, Zeiss Sigma HDP).

2.4. Adsorption studies

To examine the potential of CS/CNFs for dye removal, two anionic azo dyes, AB1 and CR, were used. The dye stock solution was prepared by dissolving 1,000 mg of each dye in 1 L of deionized water. To prepare the working solution with appropriate concentration, deionized water was used to dilute the dye stock solution. For determining AB1 and CR concentrations, the ultraviolet (UV)-visible spectrophotometry technique was used. A calibration curve was applied to calculate AB1 and CR concentrations.

The adsorption studies were conducted in batch mode. The influence of solution pH (2–8), different concentrations of adsorbent dosage (0.125–1.0 g L^{-1}), contact time (0–180 min), initial dye concentration (2.5–400 mg L^{-1}), and ionic strength (5–40 g L^{-1}) was elucidated. The effect of each parameter was analyzed while keeping the other parameters constant. The samples were shaken at agitation speed of 80 rpm for 60 min and were filtered by 0.42 mm cellulose nitrate membrane filters. To measure the residual concentrations of dyes, UV-visible spectrophotometer was used. The maximum absorbance wavelengths for AB1 and CR were 620 and 497 nm, respectively [31,32]. The solution pH was adjusted by adding negligible amount of 0.1M HCl or NaOH. The amount of dyes adsorbed per unit mass of adsorbent

(milligrams of dye per gram of adsorbent) at equilibrium time was calculated according to Eq. (1), and the dye removal efficiency was calculated using Eq. (2):

$$q_e = \frac{\left(C_0 - C_e\right)V}{m} \tag{1}$$

$$R\% = \frac{\left(C_0 - C_e\right)}{C_0} \times 100 \tag{2}$$

where C_0 and C_e denote the concentration of dyes (mg L^{-1}) at initial and equilibrium time, V is the volume of dye solution used in the adsorption experiment (L), m is the mass of adsorbent (g), and $R\%$ is removal efficiency percentage [33].

2.5. Adsorption modeling

2.5.1. Kinetic adsorption studies

Various kinetic models such as pseudo-first-order [34], pseudo-second-order [35], Avrami [36], and intra-particle diffusion models [37] were used to study the kinetics of dye adsorption on synthesized nanocomposite. The modeling equations are presented below:

Nonlinear pseudo-first-order model:

$$q_t = q_e\left(1 - e^{-(k_1 t)}\right) \tag{3}$$

Nonlinear pseudo-second-order model:

$$q_t = \frac{q_e^2 k_2 t}{1 + q_e k_2 t} \tag{4}$$

Intra-particle diffusion model:

$$q_t = k_p t^{1/2} + I \tag{5}$$

Avrami model:

$$q_t = q_e\left(1 - e^{\left(-(k_{AV} t)\right)^{n_{AV}}}\right) \tag{6}$$

where q_t is the adsorption capacity at time t (mg g^{-1}), and q_e is the adsorption capacity at equilibrium time (mg g^{-1}). k_1 is the rate constant of the pseudo-first-order model (min^{-1}), k_2 is the rate constant of the pseudo-second-order model (g mg^{-1} min^{-1}), k_p is the intra-particle diffusion rate constant (mg g^{-1} $min^{-1/2}$), I is a constant related to the boundary layer thickness (mg g^{-1}), k_{AV} is adsorption rate constant of Avrami model (min^{-1}), and n_{AV} is a constant related to the mechanism of adsorption.

2.5.2. Isotherm modeling

Different isotherm models were used which represent the correlation between equilibrium sorption of dyes and dye concentration at equilibrium time. The nonlinear forms of isotherm models including Langmuir [38], Freundlich [39], and Sips [40] are given in Eqs. (7)–(9), respectively.

$$q_e = \frac{q_m K_L C_e}{1 + K_L C_e} \tag{7}$$

$$q_e = K_F C_e^{1/n} \tag{8}$$

$$q_e = \frac{q_m \left(K_s C_e\right)^m}{1 + \left(K_s C_e\right)^m} \tag{9}$$

where q_e (mg g^{-1}) is the amount of AB1 or CR adsorbed by CS/CNFs at equilibrium time, C_e is the concentration of dye (mg L^{-1}) in solution at equilibrium time, q_m (mg g^{-1}) is the maximum adsorption capacity, K_L is the Langmuir constant (L mg^{-1}), K_F is the Freundlich constant [(mg g^{-1}) (L $mg^{-1})^{1/n}$], K_s is the affinity constant in Sips model (L mg^{-1}), and m is the dimensionless heterogeneity factor which is between 0 and 1. In case of m equal to 1, Sips model will reduce to the Langmuir equation.

In Eqs. (10) and (11), the nonlinear expression of Dubinin-Radushkevich isotherm model has been presented [41].

$$q_e = q_s \exp\left(-K_{DR} E^2\right) \tag{10}$$

$$E = \frac{1}{\sqrt{-2\beta}} \tag{11}$$

where q_s (mg g^{-1}) is a constant which is an approximate indicator of adsorption capacity, K_{DR} (mol^2 kJ^{-2}) is a constant related to the variation of free energy of adsorption. The mean of adsorption energy (E, kJ mol^{-1}) is expressed as in Eq. (11); where β (mol^2 kJ^{-2}) is a constant related to adsorption energy.

Dubinin-Radushkevich model was applied to determine if the sorption is physical or chemical in nature [42,43]. According to Eqs. (10) and (11), q_s (mg g^{-1}) is a constant which is an approximate indicator of adsorption capacity, K_{DR} (mol^2 kJ^{-2}) is a constant which is related to the variation of free energy of adsorption.

To select the best model, two parameters including root mean square error (RMSE) and coefficient of determination (R^2) showing the goodness of fit were used. The formula of these two parameters are represented in Eqs. (12) and (13), respectively.

$$\text{RMSE} = \sqrt{\frac{\sum_{i=1}^{n}\left(O_i - P_i\right)^2}{n}} \tag{12}$$

$$R^2 = \frac{\left(\sum_{i=1}^{n}\left(O_i - O_{\text{ave}}\right) \times \left(P_i - P_{\text{ave}}\right)\right)^2}{\sum_{i=1}^{n}\left(O_i - O_{\text{ave}}\right)^2 \times \sum_{i=1}^{n}\left(P_i - P_{\text{ave}}\right)^2} \tag{13}$$

where O_i is the value of observed measurement, P_i is the value of predicted measurement, n is the number of observations,

O_{ave} is the mean of observed values, P_{ave} is the mean of predicted values [6,44].

2.6. Effect of ionic strength

The effect of various NaCl concentrations (5–40 g L^{-1}) on AB1 and CR adsorption onto nanocomposite was investigated at 10 mg L^{-1} of initial dye concentrations. The changes in adsorption capacities of AB1 and CR in the presence of different NaCl concentrations were also compared.

2.7. Desorption studies

Desorption of AB1 and CR was investigated in batch mode in four successive cycles of adsorption–desorption process. Briefly, 5 mg of dye-loaded nanocomposite was suspended in 10 mL of 0.1M NaOH as eluent. Consequently, it was shaken for 60 min at 25°C at an agitation speed of 80 rpm. The desorbed nanocomposite was used as regenerated adsorbent for successive trial of adsorption–desorption process, and the concentration of filtered residual was measured by UV-visible spectrophotometer.

3. Results and discussion

3.1. Characterization of CS/CNFs

3.1.1. Zeta potential analysis

Surface charge has influence on ion affinity in aqueous solution. Particles with similar surface charge stay away from each other due to repulsive forces. In reverse conditions, particles with unlike surface charges approach each other [45]. In this study, zeta potential of nanocomposite was found to be +22.4 mv. The acidic dyes with negative charge, used in this study, were adsorbed onto nanocomposites with positive charge due to electrostatic interactions. Hailu et al. reported a change in zeta potential (to positive value) after the treatment of zeolites with cationic surfactants. The surfactant-modified zeolite exhibited effective adsorption for negatively charged Cr(VI) and acid blue dye [44]. Zhao et al. reported that semi-IPN hydrogel exhibited higher adsorption capacity for Acid Red 18 after modification with CS due to the formation of cationic amines which are in CS functional group [21]. Wang and Wang confirmed that after introducing CS into interlayer space of montmorillonite with negative surface charge, the adsorption capacity of nanocomposite for CR adsorption was greatly enhanced [23].

3.1.2. FTIR and scanning electron microscopic studies

FTIR spectra of pure and dye-loaded nanocomposites are shown in Fig. 1. The intensity and position of some peaks changed after dye adsorption which can be described due to the involvement of CS/CNF functional groups in dye adsorption [31]. The functional groups such as hydroxyl, amino, and carboxyl groups in nanocomposite can act as binding sites via electrostatic attraction [45]. In Fig. 1(a) (before adsorption), the peak at 3,290 cm^{-1} (in the range of 3,200–3,470 cm^{-1}) refers to the –OH stretch of the hydroxyl and –NH groups on nanocomposite [7]. The presence of –OH groups is due to the atmospheric water vapor adsorbed by nanocomposite

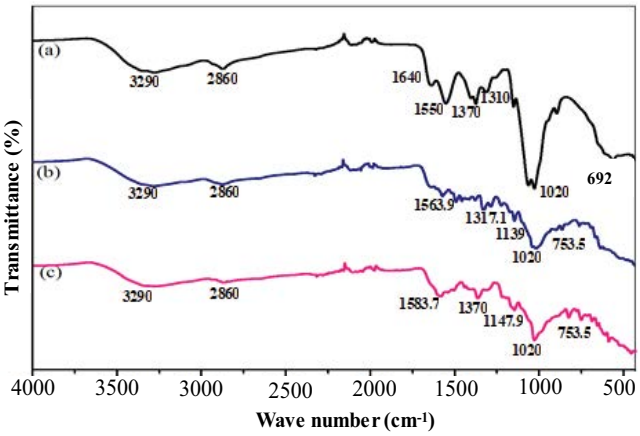

Fig. 1. FTIR spectra of CS/CNFs (a), CS/CNFs after AB1 adsorption (b), and CS/CNFs after CR adsorption (c).

material. It is in accordance with the literature reporting that carbon-nanobased materials have exhibited a broad peak at ~3,450 cm^{-1} [46,47]. The peak at 2,860 cm^{-1}, attributed to asymmetric and symmetric stretching of (C–H) bond [46], diminished after dye adsorption showing the involvement of C–H bond in dye adsorption process. The peak at 1,640 cm^{-1} is due to ester and carboxylic groups (–C=O) [48,49], and the peaks at 1,370 and 1,310 cm^{-1} corresponds to the C–N bending vibration mode while peak at 1,550 cm^{-1} is due to N=N stretching vibration mode. The peak at 1,020 cm^{-1} refers to S=O stretching vibration of sulfonic acid [50].

After adsorption, some new peaks appeared. The new peaks in the range of 590.1–664.8 cm^{-1} indicate C–C bending vibration, and a new peak at 753.5 cm^{-1} shows C–H stretching vibration [51].

The SEM and transmission electron microscopy images of CNF confirm the nanoflower structure of it (Fig. 2).

The SEM images of CS/CNFs, before and after dye adsorption, are presented in Fig. 3. The figure shows that the surface of nanocomposite has uneven surface before dye adsorption, whereas after adsorption, the particles lose their spherical shape and sinter together. In fact, interaction between CS/CNFs and dyes caused AB1 and CR to adsorb on the surface of CS/CNFs and led to a uniformity on the surface of the adsorbent [51].

3.2. Effect of solution pH

An important parameter in adsorption process is pH; therefore, the effect of different pH on AB1 and CR adsorption was examined in the pH range of 2–10 and 4–10, respectively (Fig. 5). The change of the initial solution pH in the mentioned range had insignificant effect on λ_{max} of these two dyes. λ_{max} of CR at pH 2 was found to be different from pH 4–10, but for AB1, λ_{max} was the same in the pH range of 2–10, which shows that the chemical structure of dye molecules did not change in the investigated pH range. The same observation was reported by other researchers who selected the pH range of 4–11 for CR adsorption onto Cu_2O nanoparticles [50] and pH range of 4–11 for CR adsorption onto polyaniline/Fe^0 composite nanofibers [52].

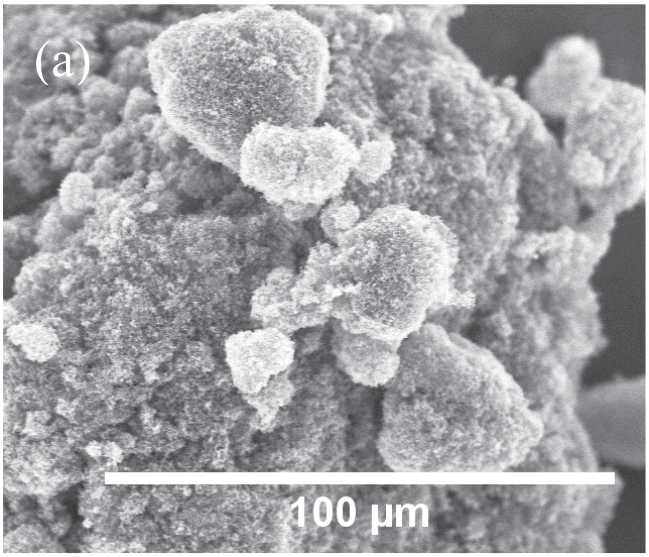

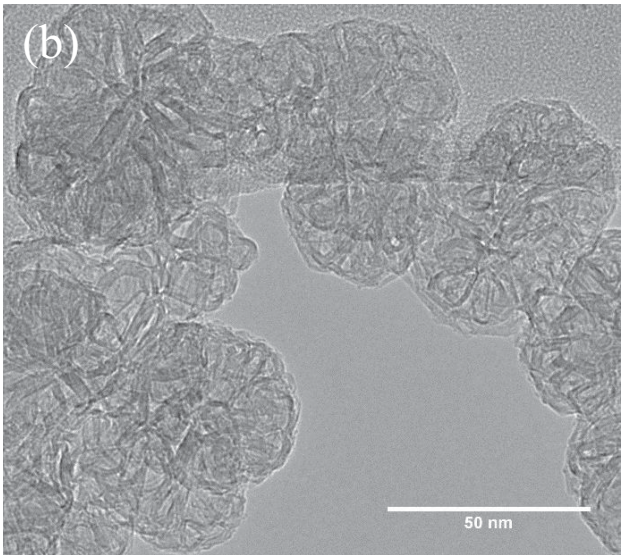

Fig. 2. Field emission scanning electron microscopy (FE-SEM) image (a) and TEM image (b) of CNFs (ref. 28).

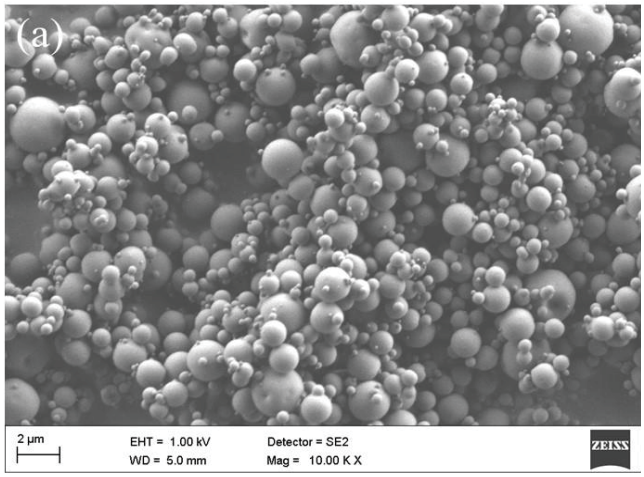

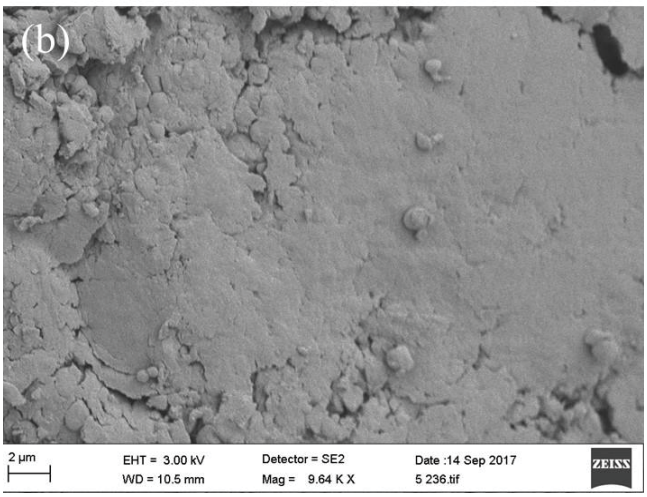

Fig. 3. FE-SEM images of CS/CNFs before adsorption (a) and CS/CNFs after adsorption (b).

At isoelectric point (pH_{IEP}), the surface charge of adsorbent becomes zero which occurred at pH 6.75 for the synthesized nanocomposite. Removal efficiency of CS/CNFs for the investigated dyes occurred maximum at pH_{IEP} (Fig. 4). Similar to this study, other researchers also confirmed that maximum removal efficiency occurred at pH_{IEP} when metal oxide nanoparticles [6] and biocomposite [45] were used as adsorbents.

The surface charge of nanocomposite varies between different pHs. At pH lower than pH_{IEP}, the surface of the adsorbent is protonated and subsequently becomes more positive. Also, with the protonation of anionic dyes and nitrogen atoms, their molecules become positively charged or neutral [53]. Therefore, electrostatic repulsion between nanocomposite and anionic dyes led to less adsorption [18,42,54]. However, at pH higher than pH_{IEP}, the surface of adsorbent becomes negatively charged. Similarly, the dye-ion surface charge becomes negative which led to less adsorption due to repulsive forces between them [42,54]. Moreover, at pH higher than pH_{IEP}, hydroxyl ions and negative-charged adsorbates compete for possessing the positively vacated sites on nanocomposite [53].

3.3. Effect of adsorbent dosage

To assess the effect of adsorbent dosage on dye removal, CS/CNFs in different dosages from 0.125 to 1 g L^{-1} were used, and the results are presented in Fig. 5. When the adsorbent dosage of nanocomposite varied from 0.125 to 0.5 g L^{-1}, removal efficiency of AB1 onto CS/CNFs increased from 53.6% to 90.9%, whereas for CR, it increased from 44.7% to 93.1%. Dye removal efficiency of AB1 and CR became constant at higher adsorbent dosage of 0.5–1 g L^{-1}, which consequently led to decreasing adsorption capacity. This could be attributed to (1) partial aggregation or overlapping of adsorption sites that results in a decrease of effective specific surface area for the adsorption [22,55] and (2) lack of sufficient dye molecules to be adsorbed by all the active

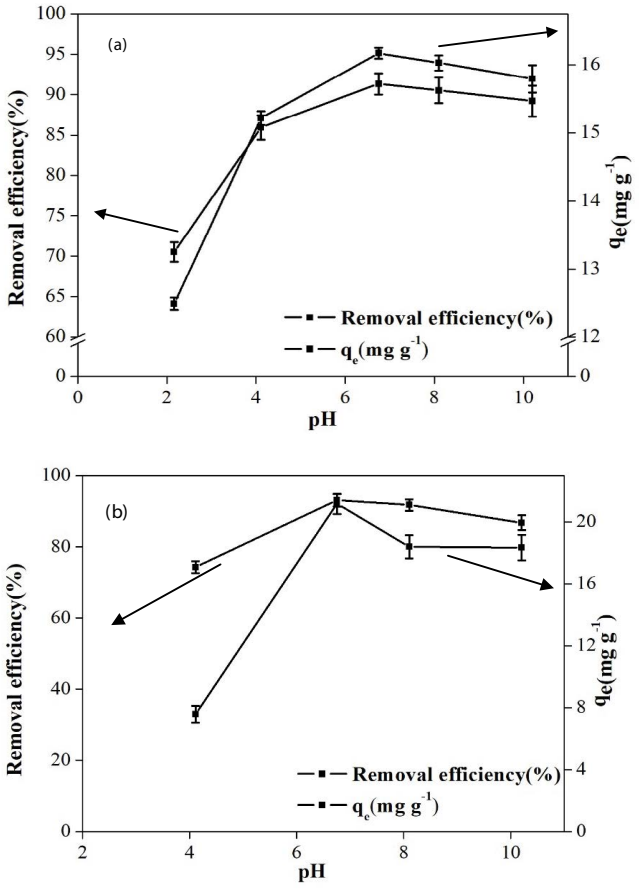

Fig. 4. Effect of solution pH on AB1 (a) and CR (b) adsorption by CS/CNFs (initial dye concentration: 10 mg L^{-1}, contact time: 60 min, temperature: 25°C, adsorbent dosage: 0.5 g L^{-1}, and initial pH 2–10).

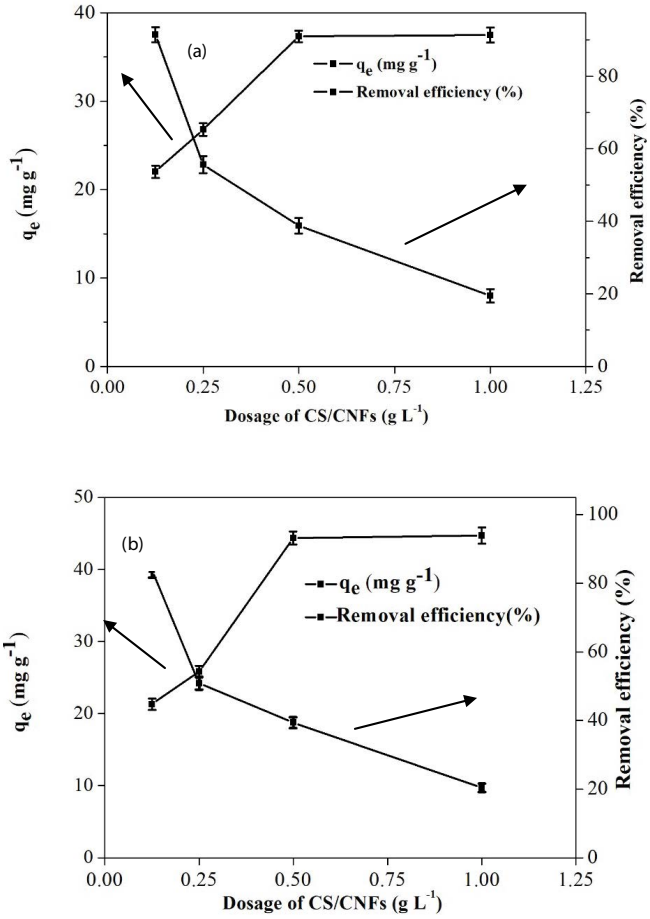

Fig. 5. Effect of adsorbent dosage on AB1 (a) and CR (b) adsorption by CS/CNFs (initial dye concentration: 10 mg L^{-1}, contact time: 60 min, temperature: 25°C, and pH 6.75).

adsorption sites which enhanced with the increase in adsorbent dosage [22]. From the results of the effects of adsorbent dosage, it was concluded that 0.5 g L^{-1} was the optimum adsorbent dosage for achieving maximum removal of dyes from water.

3.4. Effect of contact time

The effect of contact time on adsorption of AB1 and CR onto CS/CNFs was studied at initial concentration of 10 mg L^{-1} of dyes and 0.5 g L^{-1} of adsorbent dosage (Fig. 6). AB1 and CR adsorption was rapid in the beginning (up to 5 min) and slowed down thereafter. It might be attributed to the plenty of sites available on surface of the nanocomposite in the initial stage. Then, the rate of adsorption became constant because of decrease in active sites. Removal efficiencies of CS/CNFs for AB1 and CR were observed as 66% and 82%, respectively, after 10 min of contact time. Zare et al. also reported fast kinetics of CR by multiwalled carbon nanotubes with 84% removal efficiency in 10 min [19]. Equilibrium was found to be achieved in 60 min with 92% removal efficiency, and it was selected as equilibrium time for adsorption of AB1 and CR on CS/CNFs.

3.5. Effect of initial dye concentration

Removal efficiencies and equilibrium adsorption capacities as a function of initial AB1 and CR concentrations were also investigated to examine the effect of initial dye concentrations on adsorption. Initial dye concentrations of AB1 and CR were varied from 2.5 to 400 mg L^{-1} while keeping all other parameters constant (CS/CNF dosage: 0.5 g L^{-1}, temperature: 25°C ± 2°C, agitation speed: 80 rpm, contact time: 60 min, and pH: 6.75). As illustrated in Fig. 7, the increase in dye concentrations led to an increase in adsorption capacities of CR and AB1. However, for AB1, adsorption capacity reached to a plateau showing the saturation of adsorption sites on nanocomposite [31], but for CR, a plateau was not reached. These results suggest that there are still adsorption sites which can be occupied by CR molecules.

3.6. Kinetic experiments

To investigate the mechanism of adsorption and analyze the experimental data, different kinetic models (e.g., pseudo-first-order, pseudo-second-order, intra-particle diffusion, and Avrami models) were applied [19,22]. These models were

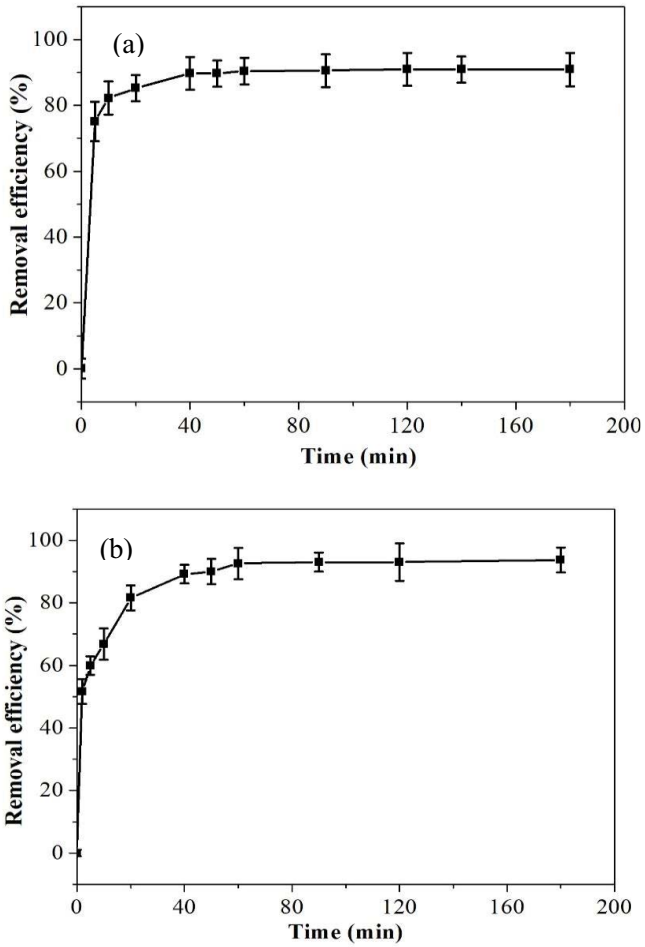

Fig. 6. Effect of contact time on AB1 (a) and CR (b) adsorption by CS/CNFs (initial dye concentration: 10 mg L^{-1}, temperature: 25°C, adsorbent dosage: 0.5 g L^{-1}, and pH 6.75).

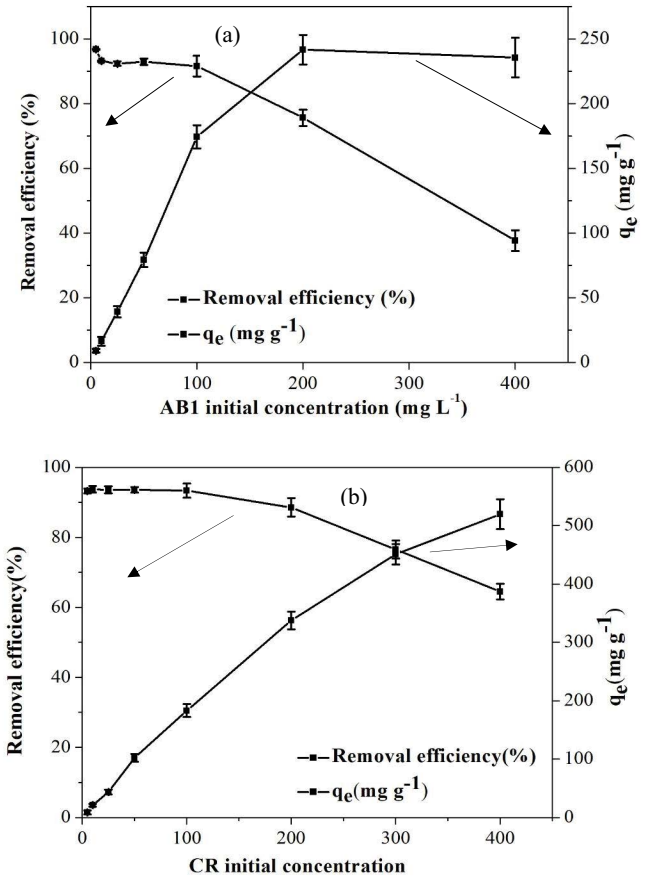

Fig. 7. Effect of initial concentration on AB1 (a) and CR (b) adsorption by CS/CNFs (contact time: 60 min, temperature: 25°C, adsorbent dosage: 0.5 g L^{-1}, and pH 6.75).

fitted to the experimental data of AB1 and CR adsorption, and the results are presented in Fig. 8. To select the best fitting model, two parameters, RMSE and R^2, were applied. The kinetic parameters are presented in Table 1. Pseudo-second-order model was better fitted to the experimental data of AB1 and CR adsorption exhibiting highest R^2 values and lowest RMSEs. Pseudo-second-order kinetic model was also found to be the most applicable model by other researchers for CR adsorption onto multiwalled carbon nanotubes [19,55] and natural zeolites [19,55]. Similar results were reported for the adsorption kinetics of various pollutants onto activated carbon cloth [56,57].

The intra-particle diffusion model was also applied to study the dynamics of adsorption process. Besides surface adsorption, diffusion into pores is also important in adsorption mechanism. According to Eq. (5), the intercept in the plot of q_t vs. $t^{1/2}$, showing the thickness of the boundary layer, is not zero. If the intercept, I, is zero, pore diffusion is the sole controlling factor; otherwise, except pore diffusion, sorption on the surface is also a dominant factor in kinetic process [42,55]. The larger the I value, the greater the contribution of surface adsorption [42,55]. The plot of q_t vs. $t^{1/2}$ for both dyes is shown in Fig. 9, which was found to have two distinct linear phases with high R^2 values. However, these lines do not pass through origin representing that pore diffusion is not the only dominating mechanism.

3.7. Effect of ionic strength

In dying process, suspended solids and salts such as sodium chloride are applied as a stimulator for accelerating or retarding dye adsorption process [21]. Chloride ions with negative charge could compete with the dye molecules for occupying positive sites of nanocomposite which consequently led to decreasing electrostatic attraction forces between nanocomposite and dye molecules [21,58]. The performance of the adsorption process is affected by high ionic strength [59]. Under various NaCl concentrations (5–40 g L^{-1}), the adsorption capacity of AB1 decreased from 15.91 to 13.90 mg g^{-1} and for CR it decreased from 19.91 to 12.45 mg g^{-1} (Fig. 10). The adsorption of CR was more affected than AB1 under ionic strength, which is in agreement with previous literature that reported slight change in removal efficiency of AB1 under different NaCl concentrations [31]. Zhao et al. also reported the negative impact of Cl^- ions on adsorption of Acid Red 18 on CS-based semi-IPN hydrogel composite [21].

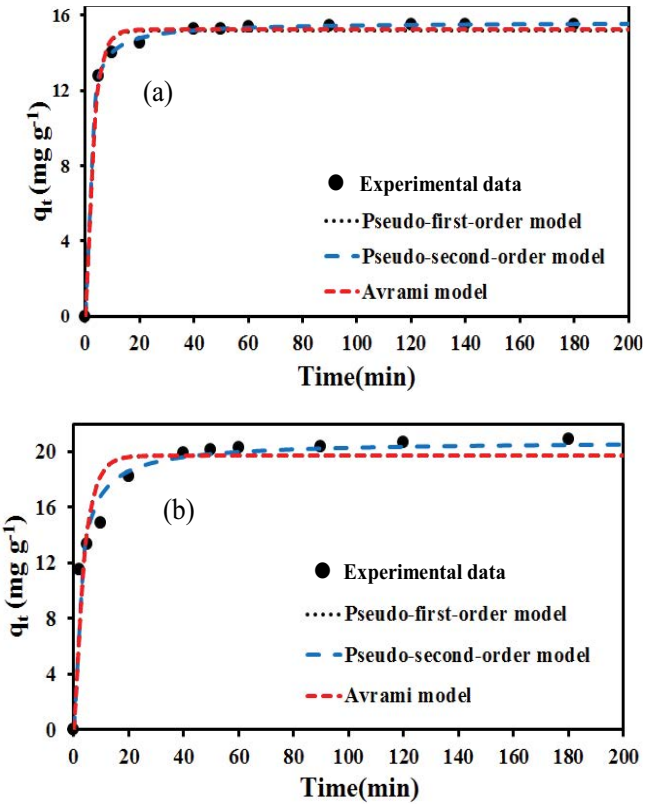

Fig. 8. Kinetic studies of AB1 (a) and CR (b) adsorption by CS/CNFs.

Table 1
Kinetic parameters for AB1 and CR ions onto the CS/CNFs

Kinetic models	Parameters		
	Variables	Value (AB)	Value (CR)
Pseudo-first-order model	$q_{e(exp)}$, mg g^{-1}	15.48	20.93
	k_1, min^{-1}	0.34	0.26
	$q_{e(cal)}$, mg g^{-1}	15.20	19.71
	RMS	0.34	1.64
	R^2	0.99	0.96
Pseudo-second-order model	$q_{e(exp)}$, mg g^{-1}	15.48	20.93
	k_2, (g mg^{-1} min^{-1})	0.05	0.02
	$q_{e(cal)}$, mg g^{-1}	15.60	20.75
	RMSE	0.08	0.89
	R^2	0.99	0.98
Avrami model	q_e, mg g^{-1}	15.48	20.93
	k_{av}, min^{-1}	0.11	0.17
	n_{av}	2.93	1.52
	$q_{e(cal)}$, mg g^{-1}	15.23	19.47
	RMSE	0.35	1.64
	R^2	0.99	0.96

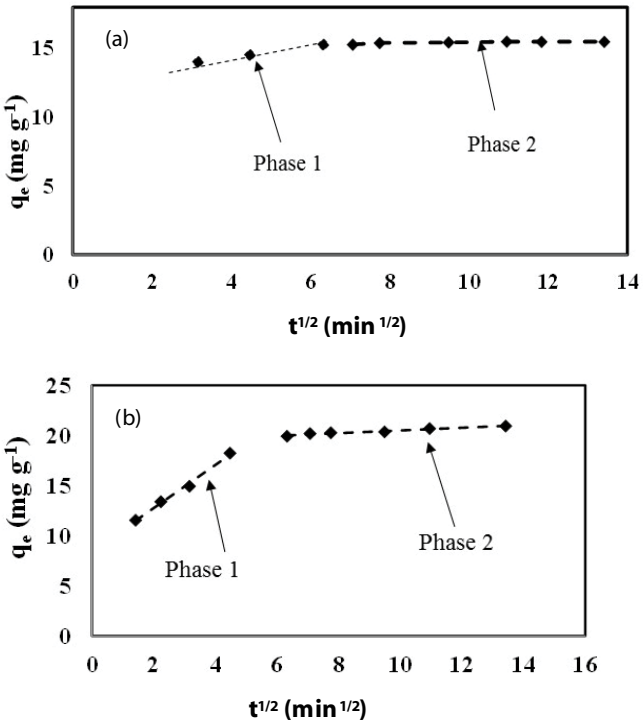

Fig. 9. Intra-particle diffusion model for AB1 (a) and CR (b) adsorption by CS/CNFs.

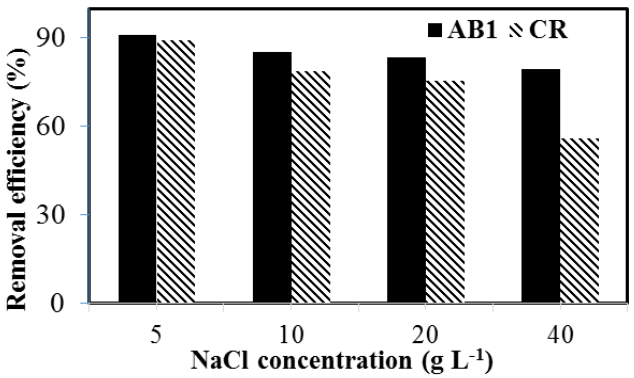

Fig. 10. Effect of ionic strength on the adsorption of AB1 and CR by CS/CNFs.

3.8. Adsorption isotherm studies

The adsorption isotherm studies were conducted to determine the maximum adsorption capacity of synthesized nanocomposite. The concentration of AB1 and CR at equilibrium time represents the distribution of dyes between the solution and adsorbent phase at equilibrium time, which can be expressed by isotherm models. At equilibrium, all active sites become saturated and a plateau was reached [31]. Isotherm models including Langmuir, Freundlich, Sips, and Dubinin-Radushkevich were applied to describe the adsorption process (Fig. 11). The maximum adsorption capacities of CS/CNFs for AB1 and CR were determined as 235.53 and 519.87 mg g^{-1}, respectively. R_L, a dimensionless constant,

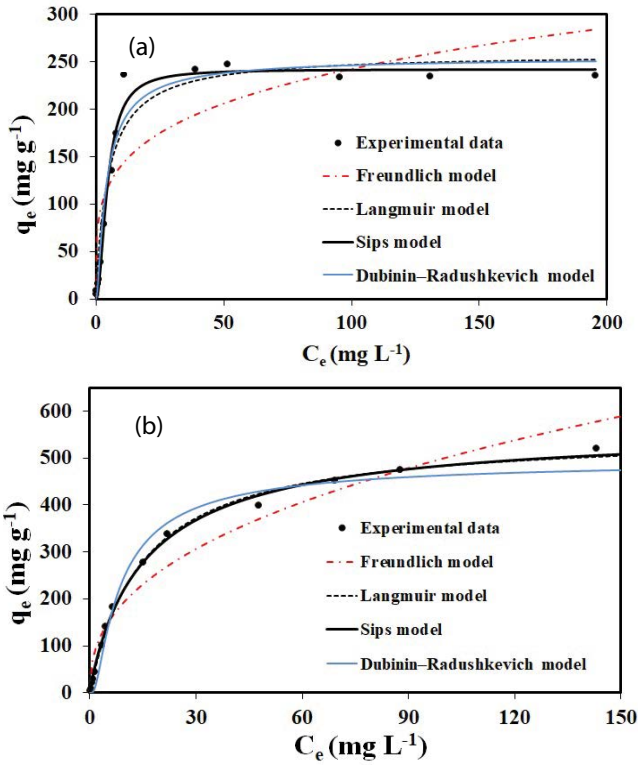

Fig. 11. Adsorption isotherm of AB1 (a) and CR (b) by CS/CNFs.

is calculated by the following equation and is applied to evaluate whether the adsorption process is favorable:

$$R_L = \frac{1}{1 + K_L C_0} \tag{14}$$

where K_L is Langmuir constant (L mg^{-1}) and C_0 is the initial concentration (mg L^{-1}). For q_m, the value of R_L was in the range of 0–1 showing the suitability of the adsorbent for the sorbate [60–62]. The results of four isotherm models (presented in Table 2) suggest that Sips model having higher R^2 and lower RMSE and ARE values fitted better to experimental data compared with Langmuir, Freundlich, and Dubinin-Rudushkevich models for AB1 and CR adsorption.

Synthesized nanocomposite showed superior adsorption capacity for the removal of CR and AB1 compared with different adsorbents used by other researchers (Table 3).

3.9. Thermodynamic studies

For determining the thermodynamic parameters, namely, change in Gibbs free energy (ΔG^0), enthalpy (ΔH^0), and entropy (ΔS^0), the following equations were used [63]:

$$K_c = \frac{C_A}{C_S} \tag{15}$$

$$\ln K_c = \frac{\Delta S^\circ}{R} - \frac{\Delta H^\circ}{RT} \tag{16}$$

$$\Delta G^\circ = \Delta H^\circ - T\Delta S^\circ \tag{17}$$

where R (8.314 J mol^{-1} K^{-1}) is a gas constant, T is absolute temperature in Kelvin, C_A is the amount of dye adsorbed on CS/CNFs at equilibrium time (mg g^{-1}), C_S is the equilibrium concentration of the dye in the solution (mg L^{-1}), and K_c (L g^{-1}) is the standard thermodynamic equilibrium constant. The slope and intercept of the plot lnK_c vs. 1/T can be used for estimating ΔH^0 and ΔS^0. As it is exhibited in Table 4, the value of ΔH^0 is positive indicating the adsorption of CR and AB1

Table 2
Isotherm parameters for AB1 and CR ions onto the CS/CNFs

Freundlich					
pollutant	K_F(mg g^{-1}) (L mg^{-1})$^{1/n}$	n	RMSE		R^2
AB1	81.75	4.23	47.01		0.89
CR	77.35	2.46	39.14		0.97
Langmuir					
pollutant	q_m (mg g^{-1})	K_L (L mg^{-1})	RMSE		R^2
AB1	259.13	0.20	20.63		0.97
CR	553.12	0.06	10.15		0.99
Sips					
pollutant	q_m (mg g^{-1})	K_s (L mg^{-1})	RMSE	ARE	R^2
AB1	242.62	0.06	11.96	13.19	0.99
CR	568.98	0.07	10.01	18.84	0.99
Dubinin-Radushkevich					
pollutant	q_m (mg g^{-1})	β	E (kJ mol^{-1})	RMSE	R^2
AB1	254.64	1.40	0.59	16.19	0.98
CR	497.67	2.89	0.41	23.86	0.99

Table 3
Adsorption capacities of different adsorbents for dye removal from aqueous solution

Adsorbent	Pollutant	pH	Temperature (°C)	q_m (mg g^{-1})	Ref.
Activated sulfidogenic sludge	CR	3.5	20	238.90	8
Multiwalled carbon nanotubes	CR	11	25	231.80	18
CS/organo-montmorillonite	CR	4	30	290.80	23
Magnetic SiO_2@$CoFe_2O_4$ nanocomposite	AB1	2	25	130.74	31
Acid-treated pine cone	CR	3.5	30	40.19	32
Polyaniline/Fe^0	CR	7	25	142.69	54
Fly ash	AB1	5	20	18.94	55
Natural zeolites modified with *N*,*N*-dimethyl dehydroabietylamine oxide	CR	6	30	69.94	57
Pine cone	AB26	2	25	62.89	66
CS/CNFs	CR	6.75	25	519.87	This study
CS/CNFs	AB1	6.75	25	235.53	This study

Table 4
Thermodynamic parameters for the adsorption of AB1 and CR by CS/CNFs

Temperature (°C)	Thermodynamic parameters		
	ΔG^0 (kJ mol^{-1})	ΔH^0 (kJ mol^{-1})	ΔS^0 (J mol^{-1} K^{-1})
AB1			
25	−6.83	29.52	122.04
35	−8.05		
45	−9.27		
CR			
25	−3.81	36.12	134.02
35	−5.15		
45	−6.49		

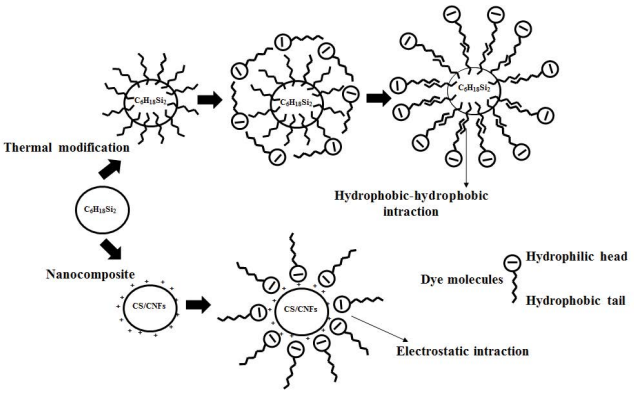

Fig. 12. Mechanism of dye adsorption onto CS/CNFs.

onto CS/CNFs is endothermic processes. This revealed that higher temperatures were more favorable for the adsorption process. The positive values of ΔS^0 in this study are the indication of irreversible adsorption and exhibited the sorption stability. Also, the positive value of ΔS^0 exhibits increased randomness during the adsorption of dyes on CS/CNF surface [63,64].

If physisorption is the dominant mechanism, then ΔG^0 values should be between –20 and 0 kJ mol^{-1}, whereas in case of chemisorption, ΔG^0 values should be between –400 and –80 kJ mol^{-1} [63]. In this study, ΔG^0 values for AB1 and CR adsorption on CS/CNFs were –6.83 and –3.81 kJ mol^{-1}, respectively; therefore, physisorption can be considered as the dominant mechanism.

3.10. Adsorption mechanism

Dye removal could be explained through the contribution of multiple mechanisms, depicted in Fig. 12. From the zeta potential value, the outer surface charge of nanocomposite is positive. Therefore, the negatively charged head of anionic dye molecules electrostatically interact with positively charged surface of CS/CNFs or there is attraction between positively charged functional group on the adsorbent surface and the anionic dye molecules [65]. The other possible mechanisms are hydrophobic interactions of nonpolar tail of dye molecules comprising long alkyl chain and the surface of CS/CNFs which becomes more hydrophobic after thermal modification [18,66]. Another dominating mechanism could be explained by hydrogen bonding having a more important role at lower pH because both CS/CNFs and two kinds of dyes become protonated and act more as donor and receptor of hydrogen atoms [66]. The intensity of absorption band at 3,290 and 2,860 cm^{-1} (Fig. 1), corresponding to stretching vibrations of O–H and C–H, has decreased after dye adsorption. It confirmed the hydrogen bond between hydroxyl groups of nanocomposite and the amine groups of dye molecules.

3.11. Regeneration of CS/CNFs

Reusability of synthesized nanocomposite is of great interest from environmental and economical point of view. Regeneration study was conducted up to four cycles with the saturated adsorbent. In the first cycle of adsorption–desorption process, the recycled adsorbent showed removal

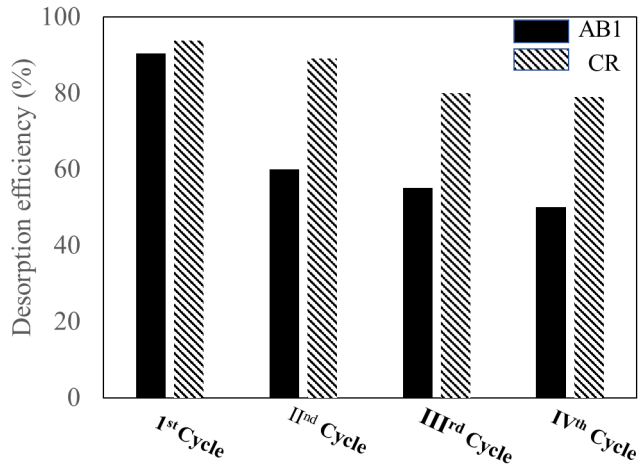

Fig. 13. Desorption studies of nanocomposite with AB1 and CR.

efficiency of 60% and 89% for AB1 and CR, respectively. However, after four cycles of adsorption–desorption process, it showed 50% and 79% removal efficiencies for AB1 and CR, respectively (Fig. 13). The regenerated nanocomposite has shown greater removal efficiency for CR compared with AB1.

4. Conclusions

A novel nanocomposite (CS/CNFs) was synthesized by spray pyrolysis method for the removal of two anionic dyes from aqueous solution. FTIR and field emission scanning electron microscopy methods were used to elucidate the physicochemical change of CS/CNFs before and after adsorption of AB1 and CR. After dye adsorption, the intensity of peaks in functional groups at 2,860 and 3,290 cm^{-1} changed. Also, some new peaks at 753.5 cm^{-1} and in the range of 590.1–664.8 cm^{-1} appeared showing the involvement of functional groups on binding dye ions. Maximum dye adsorption occurred at pH 6.75, and equilibrium was reached in 60 min. For CR and AB1 dyes, pseudo-second-order kinetic model and Sips isotherm model provided the best fit to the experimental data. According to the Langmuir isotherm model, the maximum adsorption capacities of nanocomposites were found to be 259.13 and 553.12 mg g^{-1} for AB1 and CR, respectively, at 25°C. The results of this study exhibited the potential of synthesized nanocomposite as an efficient adsorbent for the removal of toxic dyes from aqueous solution.

Acknowledgements

The author MK is grateful to Ministry of Science, Research and Technology, Iran, for the scholarship devoted to conduct her sabbatical in Department of Environmental Science, University of Eastern Finland. Also, the authors gratefully acknowledge financial support from the Academy of Finland (308062).

References

[1] C. Santhosh, V. Velmurugan, G. Jacob, S.K. Jeong, A.N. Grace, A. Bhatnagar, Role of nanomaterials in water treatment applications: a review, Chem. Eng. J., 306 (2016) 1116–1137.
[2] H.S. Rai, M.S. Bhattacharyya, J. Singh, T. Bansal, P. Vats, U. Banerjee, Removal of dyes from the effluent of textile and dyestuff manufacturing industry: a review of emerging techniques with reference to biological treatment, Crit. Rev. Environ. Sci. Technol., 35 (2005) 219–238.
[3] B. Zhao, Y. Shang, W. Xiao, C. Dou, R. Han, Adsorption of Congo red from solution using cationic surfactant modified wheat straw in column model, J. Environ. Chem. Eng., 2 (2014) 40–45.
[4] R. Han, D. Ding, Y. Xu, W. Zou, Y. Wang, Y. Li, L. Zou, Use of rice husk for the adsorption of Congo red from aqueous solution in column mode, Bioresour. Technol., 99 (2008) 2938–2946.
[5] E. Forgacs, T. Cserhati, G. Oros, Removal of synthetic dyes from wastewaters: a review, Environ. Int., 30 (2004) 953–971.
[6] S. Tangsir, L.D. Hafshejani, A. Lähde, M. Maljanen, A. Hooshmand, A.A. Naseri, H. Moazed, J. Jokiniemi, A. Bhatnagar, Water defluoridation using Al_2O_3 nanoparticles synthesized by flame spray pyrolysis (FSP) method, Chem. Eng. J., 288 (2016) 198–206.
[7] K. Rasool, D. Lee, Characteristics, kinetics and thermodynamics of Congo Red biosorption by activated sulfidogenic sludge from an aqueous solution, Int. J. Environ. Sci. Technol., 12 (2015) 571–580.
[8] Z. Cheng, L. Zhang, X. Guo, X. Jiang, T. Li, Adsorption behavior of direct red 80 and Congo red onto activated carbon/surfactant: process optimization, kinetics and equilibrium, Spectrochim. Acta A Mol. Biomol. Spectrosc., 137 (2015) 1126–1143.
[9] S. Tunc, T. Gürkan, O. Duman, On-line spectrophotometric method for the determination of optimum operation parameters on the decolorization of Acid Red 66 and Direct Blue 71 from aqueous solution by Fenton process, Chem. Eng. J., 181 (2012) 431–442.
[10] K. Vaaramaa, J. Lehto, Removal of metals and anions from drinking water by ion exchange, Desalination, 155 (2003) 157–170.
[11] T. Robinson, G. McMullan, R. Marchant, P. Nigam, Remediation of dyes in textile effluent: a critical review on current treatment technologies with a proposed alternative, Bioresour. Technol., 77 (2001) 247–255.
[12] E. Ayranci, O. Duman, In-situ UV-visible spectroscopic study on the adsorption of some dyes onto activated carbon cloth, Sep. Sci. Technol., 44 (2009) 3735–3752.
[13] E. Ayranci, O. Duman, Structural effects on the interactions of benzene and naphthalene sulfonates with activated carbon cloth during adsorption from aqueous solutions, Chem. Eng. J., 156 (2010) 70–76.
[14] O. Duman, S. Tunc, T.G. Polat, Adsorptive removal of triarylmethane dye (Basic Red 9) from aqueous solution by sepiolite as effective and low-cost adsorbent, Microporous Mesoporous Mater., 210 (2015) 176–184.
[15] O. Duman, S. Tunç, T.G. Polat, Determination of adsorptive properties of expanded vermiculite for the removal of CI Basic Red 9 from aqueous solution: kinetic, isotherm and thermodynamic studies, Appl. Clay Sci., 109 (2015) 22–32.
[16] O. Duman, S. Tunç, B.K. Bozoğlan, T.G. Polat, Removal of triphenylmethane and reactive azo dyes from aqueous solution by magnetic carbon nanotube-κ-carrageenan-Fe_3O_4 nanocomposite, J. Alloys Compd., 687 (2016) 370–383.
[17] O. Duman, S. Tunç, T.G. Polat, B.K. Bozoğlan, Synthesis of magnetic oxidized multiwalled carbon nanotube-κ-carrageenan-Fe_3O_4 nanocomposite adsorbent and its application in cationic Methylene Blue dye adsorption, Carbohydr. Polym., 147 (2016) 79–88.
[18] X. Ren, C. Chen, M. Nagatsu, X. Wang, Carbon nanotubes as adsorbents in environmental pollution management: a review, Chem. Eng. J., 170 (2011) 395–410.
[19] K. Zare, H. Sadegh, R. Shahryari-ghoshekandi, B. Maazinejad, V. Ali, I. Tyagi, S. Agarwal, V. Kumar Gupta, Enhanced removal of toxic Congo red dye using multi walled carbon nanotubes: kinetic, equilibrium studies and its comparison with other adsorbents, J. Mol. Liq., 212 (2015) 266–271.
[20] S. Chatterjee, M.W. Lee, S.H. Woo, Adsorption of Congo red by chitosan hydrogel beads impregnated with carbon nanotubes, Bioresour. Technol., 101 (2010) 1800–1806.

[21] S. Zhao, F. Zhou, L. Li, M. Cao, D. Zuo, H. Liu, Removal of anionic dyes from aqueous solutions by adsorption of chitosan-based semi-IPN hydrogel composites, Composites Part B, 43 (2012) 1570–1578.
[22] Q. Du, J. Sun, Y. Li, X. Yang, X. Wang, Z. Wang, L. Xia, Highly enhanced adsorption of Congo red onto graphene oxide/chitosan fibers by wet chemical etching off silica nanoparticles, Chem. Eng. J., 245 (2014) 99–106.
[23] L. Wang, A.Q. Wang, Removal of Congo red from aqueous solution using a chitosan/organo-montmorillonite nanocomposite, J. Chem. Technol. Biotechnol., 82 (2007) 711–720.
[24] S.-h. Wang, L. Shen, W.-D. Zhang, Y.-J. Tong, Preparation and mechanical properties of chitosan/carbon nanotubes composites, Biomacromol., 6 (2005) 3067–3072.
[25] W. Yang, Y. Wang, J. Li, X. Yang, Polymer wrapping technique: an effective route to prepare Pt nanoflower/carbon nanotube hybrids and application in oxygen reduction, Energy Environ. Sci., 3 (2010) 144–149.
[26] T.T. Kodas, M.J. Hampden-smith, Aerosol Processing of Materials, John Wiley, New York, 1999.
[27] A. Lahde, J. Raula, E.I. Kauppinen, W. Watanabe, P.P. Ahonen, D.P. Brown, Aerosol synthesis of inhalation particles via a droplet-to-particle method, Part. Sci. Technol., 24 (2006) 71–84.
[28] M. Miettinen, J. Hokkinen, T. Karhunen, T. Torvela, C. Pfüller, M. Ramsteiner, U. Tapper, A. Auvinen, J. Jokiniemi, A. Lähde, Synthesis of novel carbon nanostructures by annealing of silicon-carbon nanoparticles at atmospheric pressure, J. Nanopart. Res., 16 (2014) 2168.
[29] A. Lahde, J.R. Aula, E.I. Kauppinen, Simultaneous synthesis and coating of salbutamol sulphate nanoparticles with l-leucine in the gas phase, Int. J. Pharm., 358 (2008) 256–262.
[30] J.H. Byeon, H.-K. Kim, D.H. Thompson, J.T. Roberts, Aerosol-based fabrication of modified chitosans and their application for gene transfection, ACS Appl. Mater. Interfaces, 6 (2014) 4597–4602.
[31] S. Chella, E. Daneshvar, P. Kollu, S. Peräniemi, A. Nirmala Grace, A. Bhatnagar, Magnetic SiO_2@$CoFe_2O_4$ nanoparticles decorated on graphene oxide as efficient adsorbents for the removal of anionic pollutants from water, Chem. Eng. J., 322 (2017) 427–487.
[32] S. Dawood, T.K. Sen, Removal of anionic dye Congo red from aqueous solution by raw pine and acid-treated pine cone powder as adsorbent: equilibrium, thermodynamic, kinetics, mechanism and process design, Water Res., 46 (2012) 1933–1946.
[33] M. Bhaumik, R. McCrindle, A. Maity, Efficient removal of Congo red from aqueous solutions by adsorption onto interconnected polypyrrole–polyaniline nanofibres, Chem. Eng. J., 228 (2013) 506–515.
[34] S. Lagergren, About the theory of so-called adsorption of soluble substances, Sven. Vetenskapsakad. Handingarl, 24 (1898) 1–39.
[35] Y.S. Ho, G. McKay, Pseudo-second order model for sorption processes, Process Biochem., 34 (1999) 451–465.
[36] M. Avrami, Kinetics of phase change. I General theory, J. Chem. Phys., 7 (1939) 1103–1112.
[37] J.M.W. Weber, Intraparticle diffusion during the sorption of surfactants onto activated carbon, J. Sanit. Eng. Div. Am. Soc. Civ. Eng., 89 (1963) 53–61.
[38] I. Langmuir, The adsorption of gases on plane surfaces of glass, mica and platinum, J. Am. Chem. Soc., 40 (1918) 1361–1403.
[39] H. Freundlich, Kolloidchemie, Akademischer Verlagsgeselschaft, Leipzig, Germany, 1909.
[40] R. Sips, On the structure of a catalyst surface, J. Chem. Phys., 16 (1948) 490–495.
[41] O. Kadlec, M.M. Dubinin, Comments on the limits of applicability of the mechanism of capillary condensation, J. Colloid Interface Sci., 31 (1969) 479–489.
[42] Y. Zhou, X. Liu, Y. Xiang, P. Wang, J. Zhang, F. Zhang, J. Wei, L. Luo, M. Lei, L. Tang, Modification of biochar derived from sawdust and its application in removal of tetracycline and copper from aqueous solution: adsorption mechanism and modelling, Bioresour. Technol., 8 (2017) 1–34.
[43] Y. Ji, Ions removal by iron nanoparticles: a study on solid–water interface with zeta potential, Colloids Surf. A Physicochem. Eng. Asp., 444 (2014) 1–8.
[44] S.L. Hailu, B.U. Nair, M. Redi-Abshiro, I. Diaz, M. Tessema, Preparation and characterization of cationic surfactant modified zeolite adsorbent material for adsorption of organic and inorganic industrial pollutants, J. Environ. Chem. Eng., 5 (2017) 3319–3329.
[45] E. Daneshvar, M. Kousha, M. Jokar, N. Koutahzadeh, E. Guibal, Acidic dye biosorption onto marine brown macroalgae: isotherms, kinetic and thermodynamic studies, Chem. Eng. J., 204 (2012) 225–234.
[46] M. Bahgat, A. Farghali, W. El Rouby, M. Khedr, Synthesis and modification of multi-walled carbon nano-tubes (MWCNTs) for water treatment applications, J. Anal. Appl. Pyrolysis, 92 (2011) 307–313.
[47] Z. Zhou, Y. Liu, S. Liu, H. Liu, G. Zeng, X. Tan, C. Yang, Y. Ding, Z. Yan, X. Cai, Sorption performance and mechanisms of arsenic (V) removal by magnetic gelatin-modified biochar, Chem. Eng. J., 314 (2017) 223–231.
[48] H. Donga, J. Deng, Y. Xie, C. Zhang, Z. Jiang, Y. Cheng, K. Hou, G. Zeng, Stabilization of nanoscale zero-valent iron (nZVI) with modified biochar for Cr(VI) removal from aqueous solution, J. Hazard. Mater., 332 (2017) 79–86.
[49] Z.C.B. Chen, Sorption of naphthalene and 1-naphthol by biochars of orange peels with different pyrolytic temperatures, Chemosphere, 76 (2009) 127–133.
[50] J. Shu, Z. Wang, Y. Huang, N. Huang, C. Ren, W. Zhang, Adsorption removal of Congo red from aqueous solution by polyhedral Cu_2O nanoparticles: kinetics, isotherms, thermodynamics and mechanism analysis, J. Alloys Compd., 633 (2015) 338–346.
[51] S. Shoukat, H.N. Bhatti, M. Iqbal, S. Noreen, Mango stone biocomposite preparation and application for crystal violet adsorption: a mechanistic study, Microporous Mesoporous Mater., 239 (2017) 180–189.
[52] M. Bhaumik, R.I. McCrindle, A. Maity, Enhanced adsorptive degradation of Congo red in aqueous solutions using polyaniline/Fe^0 composite nanofibers, Chem. Eng. J., 260 (2015) 716–729.
[53] D. Suna, X. Zhanga, Y. Wub, X. Liua, Adsorption of anionic dyes from aqueous solution on fly ash, J. Hazard. Mater., 181 (2010) 335–342.
[54] S.L. Hailu, B.U. Naira, M. Redi-Abshiro, I. Diaz, M. Tessema, Preparation and characterization of cationic surfactant modified zeolite adsorbent material for adsorption of organic and inorganic industrial pollutants, J. Environ. Chem. Eng., 5 (2017) 3319–3329.
[55] S. Liu, Y. Ding, P. Li, K. Diao, X. Tan, F. Lei, Y. Zhan, Q. Li, B. Huang, Z. Huang, Adsorption of the anionic dye Congo red from aqueous solution onto natural zeolites modified with N,N-dimethyl dehydroabietylamine oxide, Chem. Eng. J., 48 (2014) 135–144.
[56] O. Duman, E. Ayranci, Attachment of benzo-crown ethers onto activated carbon cloth to enhance the removal of chromium, cobalt and nickel ions from aqueous solutions by adsorption, J. Hazard. Mater., 176 (2010) 231–238.
[57] O. Duman, E. Ayranci, Adsorptive removal of cationic surfactants from aqueous solutions onto high-area activated carbon cloth monitored by in situ UV spectroscopy, J. Hazard. Mater., 174 (2010) 359–367.
[58] A. Aguedach, S. Brosillon, J. Morvan, E.K. Lhadi, Influence of ionic strength in the adsorption and during photocatalysis of reactive black 5 azo dye on TiO_2 coated on non woven paper with SiO_2 as a binder, J. Hazard. Mater., 150 (2008) 250–256.
[59] X. Xu, B.-Y. Gao, X. Tan, Q.-Y. Yue, Q.-Q. Zhong, Q. Li, Characteristics of amine-crosslinked wheat straw and its adsorption mechanisms for phosphate and chromium (VI) removal from aqueous solution, Carbohydr. Polym., 84 (2011) 1054–1060.
[60] Y. Yang, G. Wang, B. Wang, Z. Li, X. Jia, Q. Zhou, Y. Zhao, Biosorption of Acid Black 172 and Congo Red from aqueous solution by nonviable Penicillium YW 01: kinetic study,

equilibrium isotherm and artificial neural network modeling, Bioresour. Technol., 102 (2011) 828–834.
[61] K.R. Hall, L.C. Eagleton, A. Acrivos, T. Vermeulen, Pore- and solid-diffusion kinetics in fixed-bed adsorption under constant-pattern conditions, Ind. Eng. Chem. Fundam., 5 (1966) 212–223.
[62] A. Bhatnagar, E. Kumar, M. Sillanpää, Nitrate removal from water by nano-alumina: characterization and sorption studies, Chem. Eng. J., 163 (2010) 317–323.
[63] N.M. Mahmoodi, B. Hayati, M. Arami, C. Lan, Adsorption of textile dyes on Pine Cone from colored wastewater: kinetic, equilibrium and thermodynamic studies, Desalination, 268 (2011) 117–125.
[64] X. Zhu, Y. Liu, F. Qian, C. Zhou, S. Zhang, J. Chen, Preparation of magnetic porous carbon from waste hydrochar by simultaneous activation and magnetization for tetracycline removal, Bioresour. Technol., 154 (2014) 209–214.
[65] M.C. Ncibi, M. Sillanpää, Mesoporous carbonaceous materials for single and simultaneous removal of organic pollutants: activated carbons vs. carbon nanotubes, J. Mol. Liq., 207 (2015) 237–247.
[66] M.A. Awan, S.S. Shah, Hydrophobic interaction of amphiphilic hemicyanine dyes with cationic and anionic surfactant micelles, Colloids Surf. A Physicochem. Eng. Asp., 122 (1997) 97–101.